Spin-phonon coupling in antiferromagnetic $Bi_2Sr_2CoO_{6+\delta}$: An infrared reflectance study

H. C. Hsu,[1,2] F. C. Chou,[2,3] K. Koyama,[4] K. Watanabe,[4] and H. L. Liu[1,*]
[1]*Department of Physics, National Taiwan Normal University, Taipei 11677, Taiwan*
[2]*Center for Condensed Matter Sciences, National Taiwan University, Taipei 10617, Taiwan*
[3]*National Synchrotron Radiation Center, HsinChu 30076, Taiwan*
[4]*High Field Laboratory for Superconducting Materials, Institute for Material Research, Tohoku University, Sendai 980-8577, Japan*
(Received 18 July 2008; revised manuscript received 2 February 2009; published 14 April 2009)

The *ab*-plane infrared and optical reflectance of single-crystal $Bi_2Sr_2CoO_{6+\delta}$ $(0.4<\delta<0.5)$ have been measured over a wide frequency range (50–55000 cm^{-1}) and at temperatures between 20 and 330 K. The room-temperature infrared spectrum displays an insulating characteristic. The optical gap determined from the infrared conductivity (~0.53 eV) is consistent with thermal activation energy from dc transport measurements. Upon passing through the 265 K antiferromagnetic ordering transition, a softening of the phonon mode near 205 cm^{-1} correlates well with the temperature-dependent normalized square of the sublattice magnetization. Furthermore, the magnetic-order-induced splitting of the phonon modes at about 238 and 376 cm^{-1} is observed. Additionally, the phonon mode at about 588 cm^{-1} exhibits a Fano-type line shape. Since no appreciable structural change was detected at low temperatures in x-ray diffraction studies, all of these observables suggest a complex nature of spin-phonon coupling in this material.

DOI: 10.1103/PhysRevB.79.155109 PACS number(s): 75.50.Ee, 78.30.−j

I. INTRODUCTION

Layered cobalt oxide $Bi_2Sr_2CoO_{6+\delta}$ has attracted attention because it is isostructural to the cuprate superconductor $Bi_2Sr_2CuO_{6+\delta}$. While $Bi_2Sr_2CuO_{6+\delta}$ is characterized by a network of CuO_2 planes and a transition temperature (T_c) of 10 K, $Bi_2Sr_2CoO_{6+\delta}$ contains CoO_2 planes with nonsuperconducting behavior. Furthermore, depending on the oxygen content, $Bi_2Sr_2CoO_{6+\delta}$ exhibits a series of surprising electronic and magnetic properties.[1–3] When δ is close to 0.5, the Co ions have a formal oxidation state of 3+. The material shows insulating behavior and antiferromagnetic ordering below ~250 K. The $\delta\sim0.25$ crystal has equal numbers of Co^{2+} and Co^{3+} and shows ferromagnetic behavior with a Curie temperature of $T_C\sim100$ K. Its unexpected insulating ground state is due to the charge ordering of the Co^{2+} and Co^{3+}. For crystals with $0.25<\delta<0.5$, there is a strong tendency toward a phase separation in hole-rich Co^{3+} (antiferromagnetic) and hole-poor Co^{2+}-Co^{3+} (ferromagnetic) regions.[3,4] This phase separation has been receiving a great deal of attention for its implications in the understanding of the ground state of strongly correlated electronic systems.[5]

Despite many studies of the transport and magnetic properties,[1–4] little is known about the lattice dynamics and electronic structures in $Bi_2Sr_2CoO_{6+\delta}$. Infrared and optical spectroscopic methods are an ideal bulk-sensitive tool to explore electrodynamics of correlated electron matter.[6] In this paper, we present the *ab*-plane infrared and optical reflectivity measurements of $Bi_2Sr_2CoO_{6+\delta}$ $(0.4<\delta<0.5)$ single crystals over a wide frequency range from far infrared to the near ultraviolet and at a variety of temperatures. At room temperature, the optical properties are dominated by vibrational features at low frequencies and by electronic excitations at higher frequencies. The optical gap determined from the infrared conductivity compares well with thermal activation energy from dc transport measurements. In addition, the unusual temperature dependence of phonon eigenfrequencies, dampings, and oscillator strengths of certain phonon modes involving the bending and stretching vibrations of oxygen ions in the CoO_4 squares is analyzed. It is proposed that the antiferromagnetic ordering of Co spins, which occurs below T_N, is responsible for these phonon anomalies by the spin-phonon interaction.

II. EXPERIMENT

Single crystals of $Bi_2Sr_2CoO_{6+\delta}$ were grown by the traveling solvent floating zone method. A detailed description of the sample preparation can be found elsewhere.[3] The oxygen content $(0.4<\delta<0.5)$ of the crystals was confirmed by thermogravimetric analysis. The crystals are thin platelets with dimensions of about $2\times1\times0.5$ mm^3. Magnetization measurements were performed in a superconducting quantum interference device magnetometer over the temperature range 5–350 K and at an applied field of 1 T. Figure 1 shows the

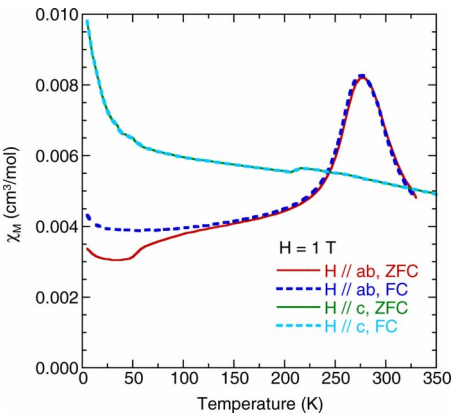

FIG. 1. (Color online) ZFC and FC magnetic susceptibilities as a function of temperature for $Bi_2Sr_2CoO_{6+\delta}$ with a magnetic field of 1 T applied along the *ab* plane and *c* axis.

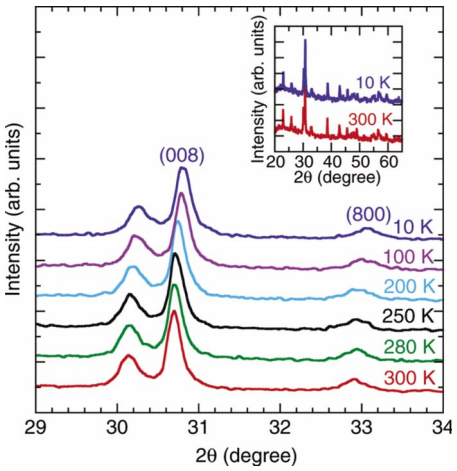

FIG. 2. (Color online) Zero-field XRD profiles of $Bi_2Sr_2CoO_{6+\delta}$ at temperature between 300 and 10 K. The inset shows the XRD spectra in the range of $20.0° < 2\theta < 65.0°$ at 300 and 10 K.

zero-field-cooled (ZFC) and field-cooled (FC) magnetic susceptibilities of $Bi_2Sr_2CoO_{6+\delta}$ with the field applied along the *ab* plane and *c* axis. The peak in the susceptibility along the *ab* plane at about 265 K is identified as the transition to antiferromagnetic order. This is in good agreement with the earlier results.[3] In addition, the susceptibility is highly anisotropic. The *c*-axis susceptibility is nearly temperature independent down to 50 K.

X-ray powder-diffraction (XRD) measurements with Cu $K\alpha$ radiation were carried out at temperatures ranging from 10 to 300 K using a Gifford-McMahon-type cryocooler cryostat and at magnetic fields up to 5 T using a cryocooled split-pair NbTi superconducting magnet.[7] From the Rietveld refinement we determined the lattice constants of the sample under investigation. The lattice parameters are $a = 5.4338(2)$ Å and $c = 23.2944(2)$ Å. Figure 2 displays the zero-field temperature dependence of XRD profiles in the diffraction angle range of $29.0° < 2\theta < 34.0°$ with step size of 0.01°. Furthermore, the inset of Fig. 2 shows the wide range of XRD data at 300 and 10 K. The XRD spectra do not change significantly with temperature, which implies that there is no structural phase transition within the temperature range investigated. Only upon cooling below 300 K, $Bi_2Sr_2CoO_{6+\delta}$ shows a decrease in the *a* and *c* lattice constants. The decrease in $a(T)$ and $c(T)$ between 10 and 300 K is about 0.0166 and 0.0736 Å, both corresponding to length changes of about 0.3%. Notably, no field-induced changes in XRD peaks were found up to 5 T, indicating that the crystallographic structure of $Bi_2Sr_2CoO_{6+\delta}$ is retained under external magnetic fields.

The near-normal optical reflectance of a single crystal of $Bi_2Sr_2CoO_{6+\delta}$ has been measured for radiation polarized parallel to the flat and mirrorlike *ab*-plane surface from 50 to 55 000 cm^{-1} on a Bruker IFS 66v Fourier transform infrared spectrometer and a Perkin-Elmer Lambda-900 spectrometer. For low-temperature measurements, the sample was mounted in a continuous flow helium cryostat equipped with a thermometer and heater near the cryostat tip, regulated by a temperature controller.

The optical properties [i.e., the complex conductivity $\sigma(\omega) = \sigma_1(\omega) + i\sigma_2(\omega)$ or dielectric constant $\epsilon(\omega) = 1 + 4\pi i\sigma(\omega)/\omega$] were calculated from a Kramers-Kronig analysis of the reflectance data.[8] Because a large frequency region was covered, a Kramers-Kronig analysis should provide reasonably accurate values of the optical constants. To perform these transformations one needs to extrapolate the reflectance at both low and high frequencies. At low frequencies the extension was done by modeling the reflectance using the Lorentz model and using the fitted results to extend the reflectance below the lowest frequency measured in the experiment. The high-frequency extrapolations were done by using a weak power-law dependence, $R \approx \omega^{-s}$ with $s \approx 1-2$.

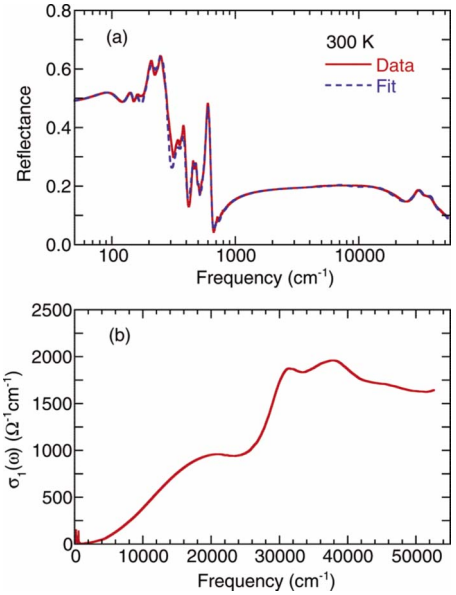

FIG. 3. (Color online) (a) Room-temperature optical reflectance spectrum (solid line) of $Bi_2Sr_2CoO_{6+\delta}$. The dashed line is the best fit using the Lorentzian model. (b) Real part of room-temperature optical conductivity spectrum of $Bi_2Sr_2CoO_{6+\delta}$.

III. RESULTS

Figure 3(a) shows the measured *ab*-plane optical reflectance of $Bi_2Sr_2CoO_{6+\delta}$ over the entire frequency range at 300 K. Note the logarithmic scale. The reflectance reveals the characteristic of an insulator at low frequencies. A number of phonon peaks are observed in the far-infrared region. At higher frequencies, the spectrum is almost dispersionless, showing only several weak electronic features. The reflectance is modeled using Lorentzian oscillators,

$$\epsilon(\omega) = \sum_{j=1}^{N} \frac{\omega_{pj}^2}{\omega_j^2 - \omega^2 - i\omega\gamma_j} + \epsilon_\infty, \tag{1}$$

where ω_j, γ_j, and ω_{pj} are the frequency, damping, and oscillator strength of the *j*th Lorentzian contribution, and ϵ_∞ is the high-frequency limit of $\epsilon(\omega)$ which includes interband transitions at frequencies above the measured range. At normal incidence, $\epsilon(\omega)$ is related to the reflectance via

TABLE I. Parameters of a Lorentzian fit for the room-temperature optical reflectance data.

Mode	ω_j (cm^{-1})	γ_j (cm^{-1})	ω_{pj} (cm^{-1})	$\Delta\epsilon_j$
1	106	59	314	8.8
2	143	21	182	1.6
3	163	20	176	1.2
4	205	38	501	6.0
5	238	35	436	3.4
6	341	63	360	1.1
7	376	31	246	0.4
8	457	19	179	0.2
9	480	35	260	0.3
10	510	18	100	0.04
11	537	20	103	0.04
12	588	37	528	0.8
13	720	41	124	0.03
	7394	2120	1553	
	18315	19984	31011	
	31058	6616	18793	
	37800	11057	26094	
	50500	23346	42224	
	ϵ_∞=	2.28		

$$R(\omega) = \left| \frac{\sqrt{\epsilon(\omega)} - 1}{\sqrt{\epsilon(\omega)} + 1} \right|^2. \quad (2)$$

Using Eqs. (1) and (2), the reflectance spectrum is well reproduced by considering 13 Lorentzian oscillators representing the phonon peaks and 5 representing the electronic interband transitions. A list of fitting parameters is given in Table I. One can also calculate the static dielectric constant from the phonon contributions as

$$\epsilon_1(0) = \sum_j \frac{\omega_{pj}^2}{\omega_j^2} + \epsilon_\infty = \sum_j \Delta\epsilon_j + \epsilon_\infty. \quad (3)$$

Our value of $\epsilon_1(0)$ of $Bi_2Sr_2CoO_{6+\delta}$ at 300 K is about 24. We are presently unaware of any microwave measurements of the static dielectric constant in $Bi_2Sr_2CoO_{6+\delta}$, so comparison with our data is not possible.

The real part of the optical conductivity $\sigma_1(\omega)$ calculated from Kramers-Kronig analysis of the reflectance is shown in Fig. 3(b). The spectrum below 800 cm^{-1} is dominated by the phonon response. Beyond the phonon regime, the conductivity gradually increases up to 18 300 cm^{-1}. An optical gap could be identified in the conductivity curve as will be discussed later. At higher frequencies, two prominent interband transitions centered at about 31 000 and 37 800 cm^{-1} are observed. While their peak strengths are somewhat sensitive to different choices for the high-frequency extrapolation in the Kramers-Kronig transformation, their shapes and positions are less affected.

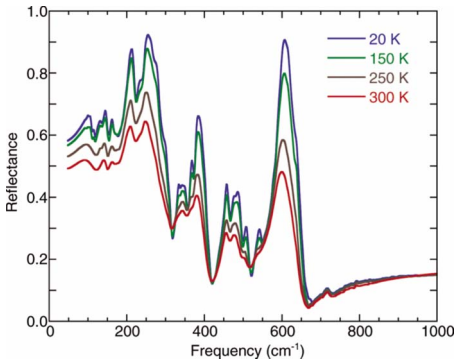

FIG. 4. (Color online) The temperature dependence of the infrared reflectance of $Bi_2Sr_2CoO_{6+\delta}$.

The temperature-dependent infrared reflectance between 50 and 1000 cm^{-1} is presented in Fig. 4. In general, the low-frequency spectral features become sharper at lower temperature, while the reflectance does not show much temperature variation above 800 cm^{-1}. Interestingly, certain phonons exhibit a peculiar behavior with decreasing temperature. This will be analyzed in more detail later. It should also be noted that no additional new phonon peaks appear below T_N, in agreement with the XRD data, indicating no significant structural change in the antiferromagnetic phase. Figure 5 shows the temperature dependence of the infrared vibrational spectra. For clarity, the temperature-dependent $\sigma_1(\omega)$ are displayed with upward baseline shifts as the temperature decreases from 300 to 20 K. The room-temperature $\sigma_1(\omega)$ exhibits 13 phonon modes, as indicated in Table I. The low-intensity broad contribution of phonon 13 around 720 cm^{-1} should be ascribed to multiphonon processes. A detailed assignment of the observed infrared phonon components was not attempted since the lattice-dynamical calculations are not presently available. Nevertheless, with decreasing temperature, most of the phonon peaks shift to higher frequency and become narrower, as usually observed in a classical anharmonic solid.[9] In contrast, phonon modes 4, 5, 7, and 12 reveal an unusual temperature dependence that cannot be explained by normal anharmonic effects. Possible mechanisms that could bring about these features are discussed below.

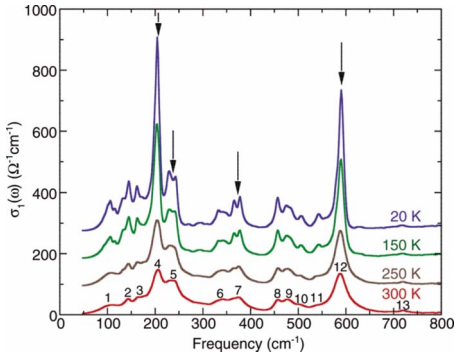

FIG. 5. (Color online) Far-infrared conductivity spectra of $Bi_2Sr_2CoO_{6+\delta}$. For clarity, the ordinate has been offset by 10% of the maximum of Y axis for the successive spectra. The phonon anomalies are indicated with an arrow.

TABLE II. Wyckoff notations, site symmetries, and irreducible representations for the atoms in $Bi_2Sr_2CoO_6$ (space group $I4/mmm$, No. 139, $Z=2$) (Ref. 13).

Atom	Wyckoff notation	Site symmetry	Irreducible representations
Bi	4*e*	C_{4v}	$A_{1g}+A_{2u}+E_g+E_u$
Sr	4*e*	C_{4v}	$A_{1g}+A_{2u}+E_g+E_u$
Co	2*a*	D_{4h}	$A_{2u}+E_u$
O(1)	4*e*	C_{4v}	$A_{1g}+A_{2u}+E_g+E_u$
O(2)	4*e*	C_{4v}	$A_{1g}+A_{2u}+E_g+E_u$
O(3)	4*c*	$D_{2h}(C_2')$	$A_{2u}+B_{2u}+2E_u$
Modes classification			
$\Gamma_{ir}=5A_{2u}+6E_u$			
$\Gamma_{Raman}=4A_{1g}+4E_g$			
$\Gamma_{silent}=B_{2u}$			
$\Gamma_{acoustic}=A_{2u}+E_u$			

IV. DISCUSSION

A. Electronic excitations

One of the striking features of the optical conductivity in $Bi_2Sr_2CoO_{6+\delta}$ ($0.4<\delta<0.5$) is the overall character of the spectra, which is insulating from 330 K down to 20 K. Most importantly, no distinct Drude component is found within the temperature and frequency ranges of our investigation. This is unlike its isostructural material of $Bi_2Sr_2CuO_6$, where a significant free-carrier contribution is due to highly mobile carriers.[10] The absent free-carrier response in $Bi_2Sr_2CoO_{6+\delta}$ suggests that the carriers are rather localized. Indeed, the temperature-dependent dc resistivity of $Bi_2Sr_2CoO_{6+\delta}$ shows thermally activated behavior[3] and follows the form

$$\rho_{dc} \propto e^{E_a/k_BT}, \tag{4}$$

where E_a is half of the optical gap. The value of the thermal activation energy in our sample is about 0.25 eV.[3] Furthermore, our oxygen-rich crystal ($0.4<\delta<0.5$) with mostly Co^{3+} ions shows two separate electronic-absorption processes, the lower-frequency bands at about 7400 and 18 310 cm^{-1}, and the higher-frequency ones at about 31 000 and 37 800 cm^{-1}. From the intersection of the extrapolated linear fit to the band edge and the abscissa, we estimate the onset of the lower-frequency electronic transition to be 0.53 eV. This onset energy corresponds roughly to the energy gap deduced from the activation energy observed in the dc transport measurements. Additionally, it has been suggested that the electronic configuration of every Co^{3+} ion in our sample is in the intermediate-spin state $t_{2g}^5e_g^1$ with $S=1$. An antiferromagnetic interaction between neighboring Co^{3+} ions can be explained in the usual way by superexchange between spins in the half filled e_g (orbital d_{z^2}) and t_{2g} (orbital d_{xy}) levels.[3] Thus, we identify the continuous increase in conductivity up to 18 310 cm^{-1} (~2.27 eV) with transitions between the Co t_{2g} and e_g orbitals. Its energy scale is also comparable to band calculations for $HoCoO_3$ and $LaCoO_3$, which yield energies of the t_{2g} and e_g states to be 2.04 and 1.93 eV, respectively.[11] Two optical excitations near 31 000 (~3.84 eV) and 37 800 cm^{-1} (~4.69 eV) can be associated with charge-transfer transitions between the O 2*p* and Co e_g states.[12]

B. Vibrational properties

We now discuss the characteristic changes in the lattice response. According to a factor group analysis, $Bi_2Sr_2CoO_6$ has a tetragonal structure with space group $I4/mmm$ in which a total of 11 infrared-active modes are expected with 5 A_{2u} modes along the *c* axis and six E_u modes in the *ab* plane (Table II).[13] The oxygen-doped sample crystallizes in the *Imma* (space group No. 74) structure.[2] Presented in Table III are the number of the expected infrared-active phonons and their symmetry. In our oxygen-rich single crystal, the room-temperature *ab*-plane $\sigma_1(\omega)$ of $Bi_2Sr_2CoO_{6+\delta}$ ($0.4<\delta<0.5$) exhibits 12 first-order phonon resonances at about 106, 143, 163, 205, 238, 341, 376, 457, 480, 510, 537, and 588 cm^{-1}. Although no detailed assignments have been made, the phonon modes of $Bi_2Sr_2CoO_{6+\delta}$ can be grouped into three fractions: low-frequency phonon bands due to Bi/Sr and CoO_4 motions ($\omega<200$ cm^{-1}), bending phonon bands at the intermediate range, and high-frequency stretching bands ($\omega>500$ cm^{-1}).[14] In the bending and stretching bands, oxygen is the primary ion that vibrates in the CoO_4 squares.

As the temperature is lowered, eight phonon modes (1–3, 6, and 8–11) show a shift of the peak position to higher frequencies and a narrowing of the resonance linewidth. As prototypical examples, Fig. 6 illustrates the frequency, damping, and oscillator strength of phonon modes 2 and 8 as a function of temperature. In a normal anharmonic solid one expects an almost temperature-independent oscillator strength, and at decreasing temperatures, the phonon frequency should increase while damping decreases. Anharmonic interactions are relevant to the high-order terms of the atomic vibrations beyond traditional harmonic terms. The temperature-dependent phonon frequency and linewidth can be written as[15]

$$\omega(T) = \omega_0\left(1 - \frac{a}{\exp(\Theta/T) - 1}\right) \tag{5}$$

and

TABLE III. Wyckoff notations, site symmetries, and irreducible representations for the atoms in $Bi_8Sr_8Co_4O_{25}$ (space group *Imma*, No. 74, $Z=4$) (Ref. 2). O-Bi refers to the oxygen atoms within the Bi-O layer, O-Sr to the oxygen atoms within the Sr-O layer, and O-Co to the oxygen atoms within the Co-O layer. The oxygen positions are distorted (i.e., there are partial occupancies).

Atom	Wyckoff notation	Site symmetry	Irreducible representations
Bi(1,5)	4*e*	$C_{2v}(C_2^z)$	$B_{1u}+B_{2u}+B_{3u}+A_g+B_{2g}+B_{3g}$
Bi(2–4)	8*i*	$C_s(\sigma^{zx})$	$2A_u+4B_{1u}+2B_{2u}+4B_{3u}+4A_g+2B_{1g}+4B_{2g}+2B_{3g}$
Sr(1,5)	4*e*	$C_{2v}(C_2^z)$	$B_{1u}+B_{2u}+B_{3u}+A_g+B_{2g}+B_{3g}$
Sr(2–4)	8*i*	$C_s(\sigma^{zx})$	$2A_u+4B_{1u}+2B_{2u}+4B_{3u}+4A_g+2B_{1g}+4B_{2g}+2B_{3g}$
Co(1)	4*e*	$C_{2v}(C_2^z)$	$B_{1u}+B_{2u}+B_{3u}+A_g+B_{2g}+B_{3g}$
Co(2)	8*i*	$C_s(\sigma^{zx})$	$2A_u+4B_{1u}+2B_{2u}+4B_{3u}+4A_g+2B_{1g}+4B_{2g}+2B_{3g}$
Co(3)	4*c*	$C_{2h}(C_2^y)$	$A_u+B_{1u}+B_{2u}+B_{3u}$
O-Bi(1)	8*h*	$C_s(\sigma^{yz})$	$2A_u+4B_{1u}+4B_{2u}+2B_{3u}+4A_g+2B_{1g}+2B_{2g}+4B_{3g}$
O-Bi(2–5)	16*j*	C_1	$3A_u+3B_{1u}+3B_{2u}+3B_{3u}+3A_g+3B_{1g}+3B_{2g}+3B_{3g}$
O-Sr(1)	4*e*	$C_{2v}(C_2^z)$	$B_{1u}+B_{2u}+B_{3u}+A_g+B_{2g}+B_{3g}$
O-Sr(2–5)	8*i*	$C_s(\sigma^{zx})$	$2A_u+4B_{1u}+2B_{2u}+4B_{3u}+4A_g+2B_{1g}+4B_{2g}+2B_{3g}$
O-Co(1,2)	16*j*	C_1	$3A_u+3B_{1u}+3B_{2u}+3B_{3u}+3A_g+3B_{1g}+3B_{2g}+3B_{3g}$
Modes classification			
$\Gamma_{ir}=43A_u+73B_{1u}+51B_{2u}+71B_{3u}$			
$\Gamma_{Raman}=72A_g+42B_{1g}+70B_{2g}+50B_{3g}$			
$\Gamma_{silent}=24A_u$			

$$\gamma(T) = \gamma_0\left(1 + \frac{b}{\exp(\Theta/T) - 1}\right), \tag{6}$$

where ω_0 and γ_0 are the harmonic frequency of the optical mode and the line broadening due to defect, respectively. Parameters a and b are the anharmonic coefficients and Θ is the Debye temperature, which can be estimated from an average of all infrared-active phonon frequencies. For the analysis of the anharmonic contributions, a Debye temperature of 497 K has been determined. The solid lines in Fig. 6 are the theoretical predictions based on Eqs. (5) and (6), which are in good agreement with the experimental data. Note that these phonon frequencies and linewidths do not show any abrupt changes at T_N. On the contrary, the oscillator strengths increase when entering the antiferromagnetic phase. At present, it is unclear if this is due to the underlying spin-phonon interaction or if this indicates that the Born effective charges are increasing in the unit cell.[15] As mentioned above, there are also important changes in certain phonon modes below T_N: (i) a saturation of the softening of phonon mode 4; (ii) a gradual splitting of phonon modes 5 and 7; and (iii) an asymmetric line shape of phonon mode 12. Similar changes in phonon modes have also been observed in other oxygen content ($0.25<\delta<0.4$) sample with $T_N\sim 150$ K.[16] Since $Bi_2Sr_2CoO_{6+\delta}$ shows no drastic temperature dependence of a crystal structure and lattice parameters, the remarkable modifications of these phonon peaks below the antiferromagnetic ordering temperature must be due to spin-phonon interactions.

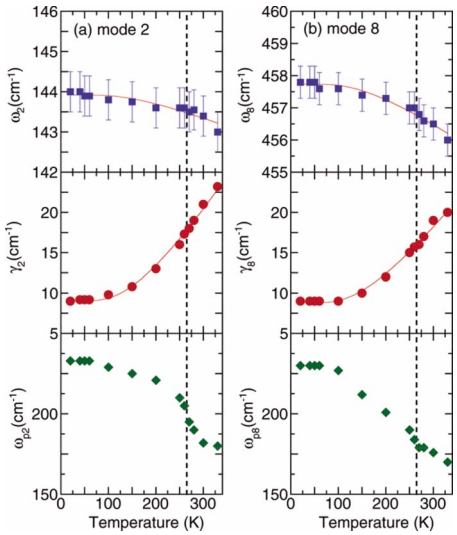

FIG. 6. (Color online) Temperature dependence of frequency, damping, and oscillator strength of phonon modes 2 and 8 in $Bi_2Sr_2CoO_{6+\delta}$. The thin solid lines are results of the fitting, taking into account the temperature-induced anharmonicity. Dotted vertical lines indicate the antiferromagnetic ordering temperature.

In the following, we address the implications of different phonon anomalies. First, the frequency versus temperature dependence for phonon mode 4 at about 205 cm^{-1} is presented in Fig. 7. It becomes clear that this phonon mode, involving bending vibrations of the oxygen ions, redshifts with decreasing temperature until 250 K. Below the antiferromagnetic ordering temperature, the redshifting saturates. More importantly, the observed phonon softening scales with the normalized square of the sublattice magnetization $[M_{sublatt}(T)/4\mu_B]^2$ (Ref. 3), revealing a strong magnetoelastic coupling. In magnetic materials, the temperature-dependent frequency change in a phonon mode can be written as[17–21]

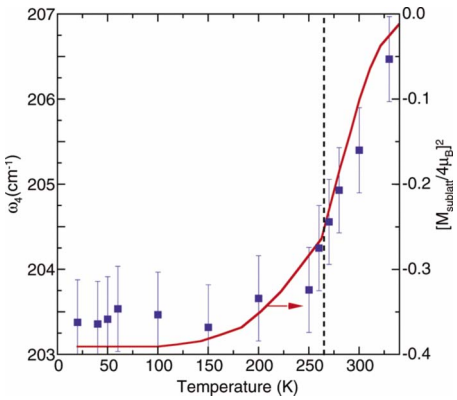

FIG. 7. (Color online) Temperature dependence of the shift of frequency of the phonon mode 4 in $Bi_2Sr_2CoO_{6+\delta}$. The solid line is the temperature-dependent normalized square of the sublattice magnetization (Ref. 3). The dotted vertical line indicates the antiferromagnetic ordering temperature.

$$\omega(T) - \omega(T_0) \equiv \Delta\omega(T) = (\Delta\omega)_{\text{latt}} + (\Delta\omega)_{\text{anh}} + (\Delta\omega)_{\text{ren}} + (\Delta\omega)_{\text{s-ph}}. \tag{7}$$

The first term is the lattice contribution and is concerned with the change in bond strengths and lengths as the unit cell contracts and expands with temperature. It is usually approximated by the Grüneisen law and assumes either a cubic crystal or an isotropically expanding or contracting lattice. The low-temperature lattice parameters derived from XRD experiments show that $Bi_2Sr_2CoO_{6+\delta}$ contracts isotropically. Phonons are expected (with regard to this term) to shift higher in frequency with decreasing temperature, as the spring constants of all vibrations tighten at low temperatures. The XRD results disagree with the softening observed in phonon mode 4. The $(\Delta\omega)_{\text{anh}}$ term accounts for the intrinsic anharmonic contribution or the anharmonicity at constant volume. In $Bi_2Sr_2CoO_{6+\delta}$, the softened phonon mode 4 saturates below T_N and suggests that the reason for such behavior is not due to anharmonicity. The third term is the renormalization contribution. This term accounts for the renormalization of electronic states that may occur near the spin ordering temperature.[22,23] $Bi_2Sr_2CoO_{6+\delta}$, however, is an insulator. Therefore, we conclude that the carrier-induced vibrational softening is not a suitable model for this system. Finally, $(\Delta\omega)_{\text{s-ph}}$ is the contribution to the change in the phonon frequency from spin-phonon interactions. The spin-phonon contribution is caused by the modulation of the exchange integral by lattice vibrations. Because the phonon mode softening in $Bi_2Sr_2CoO_{6+\delta}$ correlates with the temperature-dependent normalized square of the sublattice magnetization,[3] this term must be responsible for the softening behavior. According to the mechanism proposed by Granado *et al.*[24] the phonon softening due to the spin-phonon coupling can be expressed as

$$(\Delta\omega)_{\text{s-ph}} \approx -\frac{2}{m\omega}\frac{\partial^2 J}{\partial u^2}\left(\frac{M_{\text{sublatt}}(T)}{4\mu_B}\right)^2, \tag{8}$$

where J is the superexchange interaction, u is the displacement from equilibrium positions of the oxygen ion, and m is the oxygen mass. From the data of Fig. 7 and Eq. (8), we obtain $(\partial^2 J/\partial u^2) \approx 11.2$ mRy/Å^2. The magnitude of this value is also comparable to that obtained in the antiferromagnetic undoped manganites $R\text{MnO}_3$ (R=La, Pr, Nd, and Sm).[24,25]

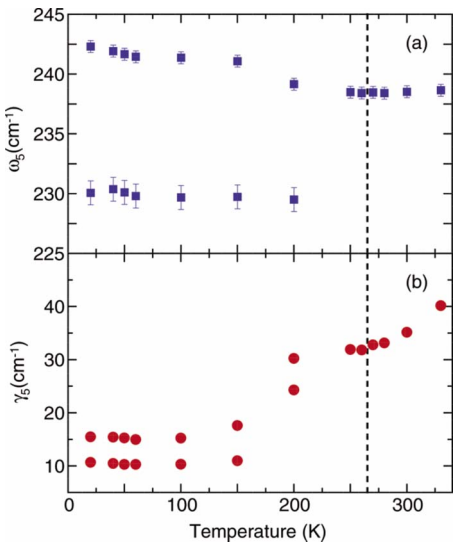

FIG. 8. (Color online) Temperature dependence of frequency and damping of the phonon mode 5 in $Bi_2Sr_2CoO_{6+\delta}$. The dotted vertical lines indicate the antiferromagnetic ordering temperature.

The second matter is the phonon splitting at the antiferromagnetic phase transition. Figures 8(a) and 8(b) show the frequency and damping of phonon mode 5 at about 238 cm^{-1} as a function of temperature. Phonon mode 7 at about 376 cm^{-1} gave qualitatively similar results. In the paramagnetic phase, the phonon frequency reveals a slight increase with decreasing temperature, as expected for an anharmonic solid. But more importantly, as is seen in Fig. 8(a), a clear splitting of the frequencies can be observed in the antiferromagnetic phase. The overall amount of splitting amount is about 12 cm^{-1} at 20 K. The temperature dependence of the damping decreases as expected from anharmoniclike phonon-phonon interactions [Fig. 8(b)]. Below T_N, the damping of the peak with lower frequency continues to decrease, as does the damping of the mode with higher frequency, and at 20 K the amount of damping is about 4% of the phonon frequency. Since no appreciable structural change was detected at low temperatures in XRD studies, the observed phonon splitting below T_N must be correlated with the antiferromagnetic spin ordering. One could speculate that spin ordering induces a small lattice distortion. This symmetry breaking is fairly weak and local (rather than long range) and does not alter the space group. That the distortion is a local phenomenon is also supported by the other center frequency vs temperature data in Fig. 6. A similar idea of a purely magnetic-order-induced phonon splitting has also been discussed by Massidda *et al.*[26] and Luo *et al.*[27] for the antiferromagnetic transition-metal monoxides (MnO and NiO).[28]

Finally, of particular interest is the temperature evolution of phonon mode 12 at about 588 cm^{-1}, as shown in Fig. 9. This phonon, mostly related to in-plane oxygen stretching

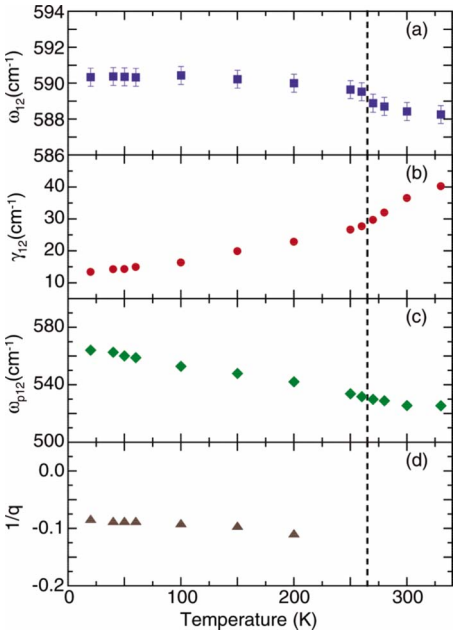

FIG. 9. (Color online) Temperature dependence of frequency, damping, oscillator strength, and asymmetry factor of the phonon mode 12 in $Bi_2Sr_2CoO_{6+\delta}$. The dotted vertical line indicates the antiferromagnetic ordering temperature.

vibrations, gradually hardens by 0.3% as the temperature decreases from 300 K down to 20 K. The hardening is due to a freezing of the lattice motion. Notably, this is the only phonon showing the asymmetric line shape at low temperatures. Such an asymmetry is fitted with the formula of Fano,[29] $\sigma(\omega)=i\sigma_0(q+i)^2/[i+x(\omega)]$, where $x(\omega)=(\omega_{12}^2-\omega^2)/\gamma_{12}\omega$, ω_{12} and γ_{12} are the resonant frequency and linewidth, and $\sigma_0=\omega_{p12}^2/\gamma_{12}q^2$ with ω_{p12} as the oscillator strength and q as the so-called asymmetry factor of the phonon mode. In the paramagnetic phase, phonon mode 12 has a symmetric (Lorentzian) line shape (i.e., $q\rightarrow\infty$). Below T_N, the asymmetric line shape develops primarily from an interaction between the lattice vibrations and a magnetic continuum. The negative value of q further indicates an interaction between the phonon mode and a temperature-dependent magnetic continuum, extending over an energy interval below the resonance frequency of the mode. It is worth noting that the big difference in energy scale between in-plane antiferromagnetic exchange interaction $J\sim150$ K (Ref. 3) and the optical phonon energy of ~850 K is an indication of the complex nature of spin-lattice interactions in this system.

V. SUMMARY

We have studied the *ab*-plane infrared and optical reflectance of $Bi_2Sr_2CoO_{6+\delta}$ ($0.4<\delta<0.5$) single crystals as a function of temperature. The infrared spectrum is characteristic of an insulator over the full temperature range of our investigation. The optical gap determined from the infrared conductivity is in reasonable agreement with the thermal activation energy from dc transport measurements. In addition, a rich phonon spectrum is observed. Eight of them shift to higher frequency and become narrower with decreasing temperature. The hardening is due to the decrease in the lattice constant on cooling and is consistent with the results of XRD measurements. At the transition into the antiferromagnetic ordered phase, a softening of the 205 cm^{-1} phonon mode follows closely the temperature-dependent normalized square of the sublattice magnetization. Such behavior is interpreted in terms of a spin-phonon coupling caused by a phonon modulation of the superexchange integral with a coupling constant of $(\partial^2 J/\partial u^2)\approx11.2$ mRy/Å^2. Based on the splitting of the 238 and 376 cm^{-1} phonon modes into a doublet, we speculate that the antiferromagnetic spin ordering induces a small local lattice distortion, hardly detectable by standard x-ray diffraction techniques. Moreover, the Fano-type shape of phonon mode at about 588 cm^{-1} suggests an interaction between lattice vibrations and a continuum of low-frequency spin excitations. These results highlight a complex coupling of spin and lattice degrees of freedom in the material.

ACKNOWLEDGMENTS

We would like to gratefully acknowledge financial support from the National Science Council of Republic of China under Grants No. NSC 95-2112-M-003-021-MY3, No. 95-2120-M-007-060, and No. 96-2120-M-007-003. The x-ray diffraction measurements in magnetic fields were carried out at the High Field Laboratory for Superconducting Materials, Institute for Materials Research, Tohoku University.

*hliu@phy.ntnu.edu.tw

[1] J. M. Tarascon, P. F. Miceli, P. Barboux, D. M. Hwang, G. W. Hull, M. Giroud, L. H. Greene, Yvon LePage, W. R. McKinnon, E. Tselepis, G. Pleizier, M. Eibschutz, D. A. Neumann, and J. J. Rhyne, Phys. Rev. B **39**, 11587 (1989).

[2] J. M. Tarascon, Y. le Page, W. R. Mckinnon, E. Tselepis, P. Barboux, B. G. Bagley, and R. Ramesh, in *High Temperature Superconductors: Relationship Between Properties, Structure and Solid-State Chemistry*, edited by J. B. Torrance *et al.*, MRS Symposia Proceedings No. 156 (Materials Research Society, Pittsburgh, PA, 1989), p. 317.

[3] K. J. Thomas, Y. S. Lee, F. C. Chou, B. Khaykovich, P. A. Lee, M. A. Kastner, R. J. Cava, and J. W. Lynn, Phys. Rev. B **66**, 054415 (2002).

[4] Y. Nagao, I. Terasaki, and T. Nakano, Phys. Rev. B **76**, 144203 (2007).

[5] E. Dagotto, T. Hotta, and A. Moreo, Phys. Rep. **344**, 1 (2001), and references therein.

[6] S. V. Dordevic and D. N. Basov, Ann. Phys. **15**, 545 (2006).

[7] K. Watanabe, Y. Watanabe, S. Awaji, M. Fujiwara, N. Kobayashi, and T. Hasebe, Adv. Cryog. Eng. **44**, 747 (1998).

[8] F. Wooten, *Optical Properties of Solids* (Academic, New York,

1972).
[9] R. A. Cowley, Adv. Phys. **12**, 421 (1963).
[10] A. A. Tsvetkov, J. Schutzmann, J. I. Gorina, G. A. Kaljushnaia, and D. van der Marel, Phys. Rev. B **55**, 14152 (1997).
[11] I. A. Nekrasov, S. V. Streltsov, M. A. Korotin, and V. I. Anisimov, Phys. Rev. B **68**, 235113 (2003).
[12] J. Zhou, P. Zheng, and N. L. Wang, J. Phys.: Condens. Matter **20**, 055222 (2008).
[13] G. Burns, G. B. Chandrashekhar, F. H. Dacol, M. W. Shafer, and P. Strobel, Solid State Commun. **67**, 603 (1988).
[14] J. Prade, A. D. Kulkarni, F. W. de Wette, U. Schroder, and W. Kress, Phys. Rev. B **39**, 2771 (1989).
[15] K.-C. Liang, H. L. Liu, H. D. Yang, W. N. Mei, and D. C. Ling, J. Phys.: Condens. Matter **20**, 275238 (2008).
[16] H. C. Hsu *et al.* (unpublished).
[17] W. Baltensperger and J. S. Helman, Helv. Phys. Acta **41**, 668 (1968).
[18] W. Baltensperger, J. Appl. Phys. **41**, 1052 (1970).
[19] P. Brüesch and F. D'Ambrogio, Phys. Status Solidi B **50**, 513 (1972).
[20] D. J. Lockwood and M. G. Cottam, J. Appl. Phys. **64**, 5876 (1988).
[21] J. M. Wesselinowa and A. T. Apostolov, J. Phys.: Condens. Matter **8**, 473 (1996).
[22] K. H. Kim, J. Y. Gu, H. S. Choi, G. W. Park, and T. W. Noh, Phys. Rev. Lett. **77**, 1877 (1996).
[23] M. N. Iliev, A. P. Litvinchuk, H.-G. Lee, C. L. Chen, M. L. Dezaneti, C. W. Chu, V. G. Ivanov, M. V. Abrashev, and V. N. Popov, Phys. Rev. B **59**, 364 (1999).
[24] E. Granado, A. García, J. A. Sanjurjo, C. Rettori, I. Torriani, F. Prado, R. D. Sánchez, A. Caneiro, and S. B. Oseroff, Phys. Rev. B **60**, 11879 (1999).
[25] J. Laverdière, S. Jandl, A. A. Mukhin, V. Yu. Ivanov, V. G. Ivanov, and M. N. Iliev, Phys. Rev. B **73**, 214301 (2006).
[26] S. Massidda, M. Posternak, A. Baldereschi, and R. Resta, Phys. Rev. Lett. **82**, 430 (1999).
[27] W. Luo, P. Zhang, and M. L. Cohen, Solid State Commun. **142**, 504 (2007).
[28] T. Rudolf, Ch. Kant, F. Mayr, and A. Loidl, Phys. Rev. B **77**, 024421 (2008).
[29] U. Fano, Phys. Rev. **124**, 1866 (1961).